Materials Today • Volume xxx, Number xx • xxxx 2021 RESEARCH

ELSEVIER

RESEARCH: Original Research

A localized glyco-editing probe for revelation of protein-specific glycan function

Siqiao Li [1,2], Anwen Mao [1], Fan Huo [4], Xiaojian Wang [3], Yuna Guo [1], Lu Liu [1], Chao Yan [4,5], Lin Ding [1,5,*], Huangxian Ju [1]

[1] State Key Laboratory of Analytical Chemistry for Life Science, School of Chemistry and Chemical Engineering, Nanjing University, Nanjing 210023, China
[2] Faculty of Basic Medical Sciences, Chongqing Medical University, Chongqing 400016, China
[3] Institute of Advanced Synthesis, School of Chemistry and Molecular Engineering, Nanjing Tech University, Nanjing 211816, China
[4] State Key Laboratory of Pharmaceutical Biotechnology, School of Life Sciences, Nanjing University, Nanjing 210023, China
[5] Chemistry and Biomedicine Innovation Center (ChemBIC), Nanjing University, Nanjing 210023, China

The ability to execute live-cell, localized glyco-editing is of pivotal importance for revolutionizing the field of glycobiology but no effective tool has been developed. We report herein the design of protein-specific glyco-editing probes, operating through localized enzyme decaging (LED), for live-cell editing of carbohydrate units on the protein of interest. The integration of aptamer recognition and molecular cloaking/uncloaking-based glyco-enzyme caging/decaging mechanism ensures the protein-specific editing. Proof-of-concept demonstration has been achieved for mucin 1 (MUC1)-specific terminal galactose/*N*-acetylgalactosamine (Gal/GalNAc) editing and sialic acid (Sia) trimming on live cells. A unique advantage of our LED strategy is the modular adaptability for performing cascade localized glyco-editing (CALOGE) manipulation through sequential aptamer docking-erasing-docking processes. Moreover, *in vivo* MUC1-specific Gal/GalNAc editing has also been realized, which enables the fluorescence visualization of Gal/GalNAc on MUC1 in murine bladder. In particular, specific trimming of MUC1-bound Sia on live cells has demonstrated, for the first time, the ability to directly reveal the significant effects of protein-specific glycoform on intracellular signaling and cell migration. These results suggest the probe as a generically applicable investigation tool for the revelation and manipulation of biological functions in association with protein-specific glycoforms.

Keywords: Aptamer; Glyco-editing enzyme; Live cell imaging; Localized enzyme decaging; Protein-specific glyco-editing probe

Introduction

Protein glycosylation is a ubiquitous, complex, and important post-translational modification in biological systems [1]. The glycosylation state of a protein, or the protein-specific glycoform, is under strict control of cellular biosynthetic machinery [2] and provides an elaborate handle for regulating the properties of protein and associated cell [3,4]. The revelation of underlying cellular processes and designated cellular functions for protein-specific glycoform is pivotal for the general understanding and full utilization of non-template-derived phenomena [5], and relies critically on the ability to execute precise editing of carbohydrate units confined to a particular protein. However, despite extensive advances in the field of glycobiology, no generically

* Corresponding author.
E-mail address: Ding, L. (dinglin@nju.edu.cn)

 https://doi.org/10.1016/j.mattod.2021.04.015

Please cite this article in press as: S. Li et al., Materials Today (2021), https://doi.org/10.1016/j.mattod.2021.04.015

applicable strategy has been established for protein-specific glyco-editing. To enable protein-specific glyco-editing, four requirements must be fulfilled: high protein-targeting selectivity, efficient glyco-editing capacity, stringent division of protein-targeting stage and glyco-editing stage to avoid off-target remodeling, flexible adaptability to various glyco-editing schemes (i.e. gain-of-carbohydrate, loss-of-carbohydrate, and transformation-of-carbohydrate).

The genetic regulation of glycosyltransferase expression level [6] as well as metabolic oligosaccharide engineering (MOE) technique [7] are currently widely used for glycan editing. However, due to the inherent lack of protein-targeting instrument in these "internal" pathways, the cell surface glycoforms are altered at the global level, resulting in, essentially, the incompetence to link observed functional property to a particular protein glycoform; further conundrums include the potential disruption of endogenous gene for genetic engineering [8] and stretched metabolic time course for MOE [9], etc. Although mutation of glycosylation sites can confine the glycoform manipulation on a given protein type [10], this operation might perturb the native structure and properties of the protein, and is basically used in the scenario of "loss-of-carbohydrate" manipulation.

As an alternative approach to edit cell surface glycans [11–13], the "external" chemoenzymatic remodeling method typically takes advantage of the promiscuous glycosyl transfer activity of an exogenous recombinant enzyme to install a carbohydrate unit on all available acceptors; no protein-targeting specificity is imposed. Although yet to be demonstrated, in principle, protein-specific glyco-editing can be achieved for this double-substrate, "gain-of-carbohydrate" scheme since the division of protein-targeting stage and glyco-editing stage can be administered by the substrate control (i.e., accessibility of donor molecule). However, the "transformation-of-carbohydrate" and "loss-of-carbohydrate" manipulations can not be straightforwardly implemented as the enzyme control (i.e., accessibility of enzymatic activity) is mandatory in these single-substrate scenarios. To our knowledge there has been only one report from our previous study where the protein-specific "transformation-of-carbohydrate" has been accomplished through inactivation/activation of glyco-enzyme catalytic center [14]; however, this type of catalytic center inactivation/activation sequence is not a predictably effective strategy in general and has to be tested on a case-by-case basis, thus undermining its versatility and utility.

To address the numerous issues in aforementioned approaches, herein we have developed protein-specific glyco-editing probes, operating through localized enzyme decaging (LED), for live-cell editing of carbohydrate units on the protein of interest. The glyco-editing probes are comprised of three components: a protein-targeting aptamer, a glyco-editing enzyme, and a removable enzyme-cloaking entity. The LED proceeds by initial aptamer recognition-guided delivery of the glyco-editing enzyme in the caged state to target protein and subsequent decaging for protein-confined, proximity catalysis-effected glyco-editing (Fig. 1). Instead of direct tampering with the enzyme catalytic center [14], the LED strategy exploits the accessibility of enzyme catalytic center as a regulatory handle and molecular cloaking/uncloaking as the adaptable caging/decaging channel [15,16], thus offering a generically applicable tool for protein-specific glyco-editing. An important feature of our LED strategy is the ability to achieve cascade localized glyco-editing (CALOGE) through the connection of distinct glyco-editing schemes (also involving different glyco-enzymes) by sequential aptamer docking-erasing-docking processes. Furthermore, the LED-based editing can be also performed *in vivo*, affording a fluorescence imaging method for protein-specific glycans in murine bladder. Importantly, through precision remodeling of glycans on live cells, the consequence of glyco-editing event can be directly tracked, thus allowing the revelation of glycan functions at the single-type protein level.

Experimental methods

Preparation of pro-editing aptamer-galactose oxidase-poly (ethylene glycol) (PEG) conjugate (A-G-SS-P)

Galactose oxidase (GO, 3.4 mg/mL, 120 μL) purified by gel filtration column and *N*-succinimidyl-3-(2-pyridyldithio)propionate (SPDP, 100 mM, 1.2 μL) were added in PBS buffer (pH 8.0, 80 μL). The mixture was incubated under continuous gentle mixing at room temperature (r.t., 25 °C) for 2 h to prepare G-SS, followed by removing excess SPDP by ultrafiltration and resuspension in PBS buffer (pH 8.0, 200 μL). Then G-SS-P was prepared by incubation of the mixture containing G-SS (1.4 mg/mL, 143 μL), mPEG2000-SH (150 mM, 50 μL), and PBS buffer (pH 8.0, 7 μL) under the same condition as that for preparing G-SS, and resuspended in PBS buffer (pH 5.5, 150 μL) after ultrafiltration purification. Finally, after incubation of G-SS-P (0.95 mg/mL, 150 μL), 0.8 mg *N*-(3-dimethylaminopropyl)-*N*-ethylcarbodiimide hydrochloride (EDC), and 0.9 mg *N*-hydroxysulfosuccinimide (Sulfo-NHS) at r.t. for 30 min to activate the carboxyl groups of GO, 3′-amino group conjugated mucin 1 (MUC1) aptamer S2.2 (Apt-NH_2, 100 μM, 40 μL) was mixed with activated G-SS-P (0.95 mg/mL, 114 μL) to prepare A-G-SS-P. The pH of mixture was adjusted to 7.5–8.0, followed by gentle mixing at r.t. for 4 h and ultrafiltration to remove unreacted Apt-NH_2. The prepared A-G-SS-P was dispersed in PBS buffer (pH 8.0, 100 μL).

Determination of enzymatic activity of GO and GO conjugates in vitro

According to the standard procedure of Amplex™ Red Gal/GO assay kit [17], 50 μL GO or GO conjugates (0.24 μg/mL in GO unit) in the presence and absence of tris(2-carboxyethyl) phosphine hydrochloride (TCEP, 2.0 mM) in Reaction Buffer (1×, 0.05 M Tris-HCl containing 1 mM $CaCl_2$, pH 7.2) was added into 96-well plates. Then, 50 μL of Reaction Buffer (1×) containing 100 μM Amplex Red Reagent, 0.2 U/mL horseradish peroxidase (HRP), and 200 μM galactose (Gal) was added to each well and the mixture was incubated at 37 °C for 1 h in the dark to avoid fluorescence quenching. The emission signal at 590 nm was measured at the excitation wavelength of 540 nm.

Monitoring of GO activity in A-G-SS-P with and without TCEP using different substrates

50 μL Reaction Buffer (1×) containing A-G-SS-P or GO (0.24 μg/mL in GO unit for substrates Gal or lactose (Lac), 4.2 μg/mL in GO unit for substrates mucin from porcine stomach (MUC2) or fixed MCF-7 cells), with and without TCEP (2.0 mM), was mixed

Please cite this article in press as: S. Li et al., Materials Today (2021), https://doi.org/10.1016/j.mattod.2021.04.015

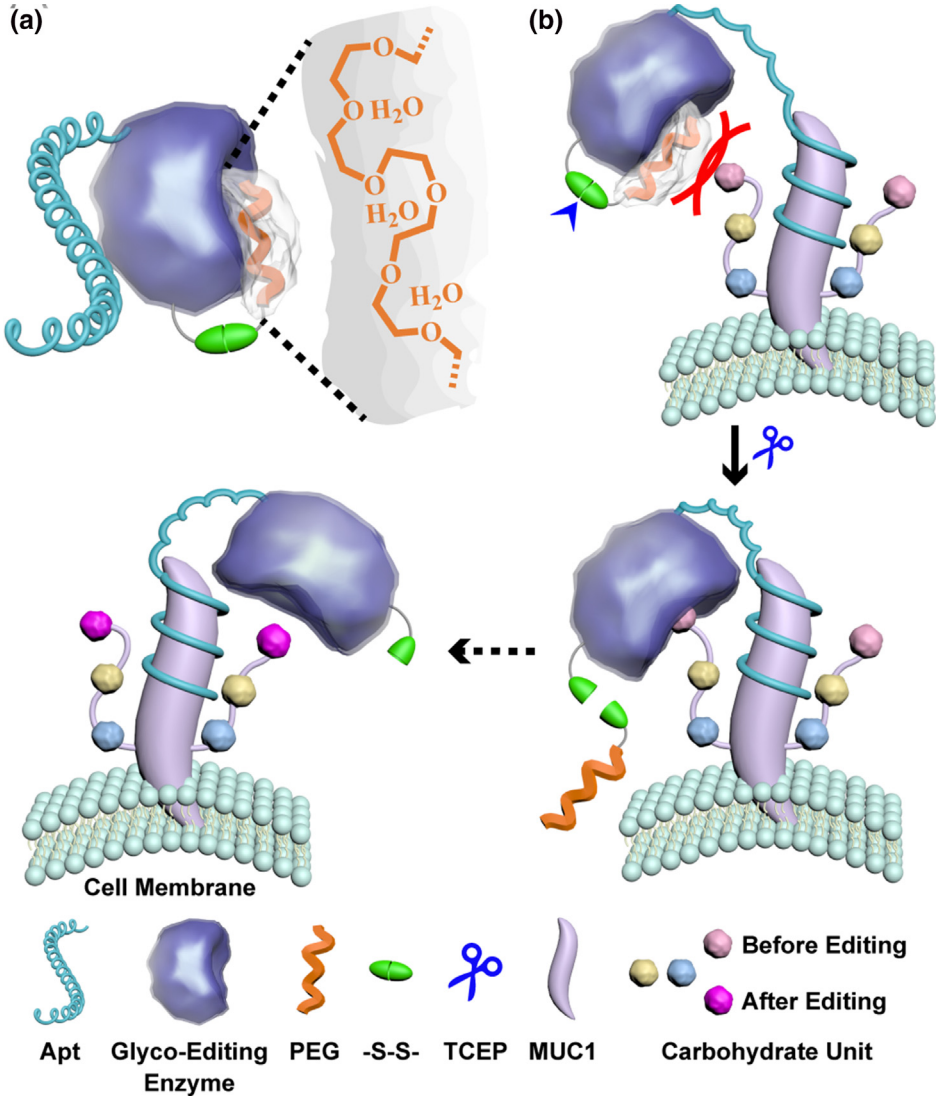

FIGURE 1

Schematic illustration of the localized enzyme decaging (LED) strategy. (a) Scheme of the pro-editing conjugate. (b) Principle of the LED strategy for precision live-cell, protein-targeted glyco-editing.

with 50 μL Reaction Buffer (1×) containing 100 μM Amplex Red Reagent, 0.2 U/mL HRP, and 200 μM Gal (or 0.4 mg/mL Lac, 0.32 mg/mL MUC2, suspending fixed MCF-7 cells with an equivalent protein concentration of 0.33 mg/mL). The reaction was proceeded at 37 °C for 1 h in the dark, and the emission signal at 590 nm was determined under 540 nm excitation.

MUC1-specific terminal galactose/N-acetylgalactosamine (Gal/GalNAc) editing by A-G-SS-P based LED strategy

MCF-7 cells were seeded at a density of 0.5×10^6 cells/mL on four-well confocal dishes and cultured overnight. After discarding the culture medium and washing cells with PBS, the cells were blocked with PBS containing 10% goat serum for 30 min and washed three times with PBS. Then the cells were incubated with A-G-SS-P (0.4 μM in GO unit) at 4 °C for 30 min, followed by washing with PBS. Then TCEP (2.0 mM in PBS) was added into each well, and the cells were incubated at r.t. for 1 h under gentle shaking. After washing with PBS, the cells were subjected to incubation with PBS at 4 °C for 30 min. After washing three times with PBS, the cells were subjected to bioorthogonal labeling with 100 μL PBS solution containing 10 mM aniline, 100 μM fluorescein-5-thiosemicarbazide (FTZ), and 5% fetal bovine serum (FBS) at 4 °C for 1 h. After washing with PBS, the FTZ fluorescence on cell membrane was imaged with confocal laser scanning microscopy (CLSM). The emission signal from 505 nm to 565 nm was collected under 495 nm excitation. The fluorescence intensities (FI) of cells were recorded by averaging of pixel readout over 10 cell contours, in triplicates.

Preparation of aptamer-neuraminidase (NEU)-PEG conjugate (A-N-SS-P)

NEU (1.0 mg/mL, 147 μL) purified by gel filtration column and SPDP (100 mM, 0.8 μL) were added in PBS buffer (pH 8.0, 52.2 μL). The mixture was incubated under continuous gentle mixing at r.t. for 2 h to prepare N-SS, followed by removing excess SPDP by ultrafiltration and resuspension in PBS buffer (pH 8.0, 200 μL). Then N-SS-P was prepared by incubation of the mixture containing N-SS (0.51 mg/mL, 143 μL),

Please cite this article in press as: S. Li et al., Materials Today (2021), https://doi.org/10.1016/j.mattod.2021.04.015

mPEG2000-SH (100 mM, 5 μL), and PBS buffer (pH 8.0, 52 μL) under the same condition as that for preparing N-SS, and resuspended in PBS buffer (pH 5.5, 150 μL) after ultrafiltration purification. Finally, after incubation the mixture of N-SS-P (0.34 mg/mL, 150 μL), 0.3 mg EDC, and 0.4 mg sulfo-NHS at r.t. for 30 min to activate the carboxyl groups of NEU, Apt-NH_2 (100 μM, 15 μL) was mixed with activated N-SS-P (0.34 mg/mL, 123 μL) to prepare A-N-SS-P. The pH of mixture was adjusted to 7.5–8.0, followed by gentle mixing at r.t. for 4 h and ultrafiltration to remove unreacted Apt-NH_2. The prepared A-N-SS-P was dispersed in PBS buffer (pH 8.0, 100 μL).

MUC1-specific sialic acid (Sia) trimming by A-N-SS-P based LED strategy

After seeding and blocking, MCF-7 cells were incubated with A-N-SS-P (1.4 μM in NEU unit) at 37 °C for 30 min, followed by washing with PBS. Then TCEP (2.0 mM in PBS) was added into each well, and the cells were incubated at r.t. for 1 h under gentle shaking. After washing with PBS, the cells were subjected to incubation with PBS at 37 °C for 30 min. After three times of washing and FITC-tagged *Sambucus nigra* agglutinin (SNA-FITC) labeling, the cells were imaged with CLSM.

Cascade localized glyco-editing (CALOGE)

After performing MUC1-specific Sia trimming using a counterpart probe, A′-N-SS-P (A′ is an extended Apt-bearing DNA strand designed to be amenable to toehold-mediated strand displacement), via the same procedure, A′-comp (10 μM) was added and allowed to incubate at 37 °C for 30 min. After washing with PBS, the cells were subjected to incubation with a mixture of Apt-conjugated GO (G-A) (0.4 μM in GO unit, prepared by conjugating NH_2-Apt and GO) and $K_4[Fe(CN)_6]$ (100 mM) in PBS buffer at 37 °C for 30 min, three-time PBS washing, and treatment with 10 mM $K_3[Fe(CN)_6]$ in PBS at 37 °C for 30 min. After three times of washing and bioorthogonal labeling with 100 μL PBS solution containing 10 mM aniline, 100 μM FTZ, and 5% FBS at 4 °C for 1 h, the cells were washed and imaged with CLSM and the emission signal from 505 nm to 565 nm was collected under 495 nm excitation.

In vivo MUC1-specific terminal Gal/GalNAc editing by A-G-SS-P based LED strategy

All procedures were in accordance with the Institutional Animal Use and Care Regulations authorized by the Model Animal Research Center of Nanjing University (MARC). Pathogen-free female C57BL/6J mice (7–8 weeks) were randomly divided into two groups: bladder group and muscle group. For bladder group, bladder irrigation was implemented by inserting a 24-gauge BD Insyte catheter through the urethra into the bladder. For muscle group, the intramuscular injection to the thigh muscles of the hind limb was performed with a 26-gauge KDL sterile syringe. Each group was further divided into three sub-groups, including A-G-SS-P sub-group, Apt control sub-group, and GO control sub-group. For each sub-group, at least 3 mice were used.

For bladder group, after anaesthetization with 4% chloral hydrate (0.20 mL/20 g), the A-G-SS-P sub-group was treated with A-G-SS-P (4.0 μM in GO unit, 50 μL) for 30 min followed by washing with PBS. After treatment with TCEP (2.0 mM in PBS, 50 μL) for 60 min, the bladder was subjected to incubation with 50 μL PBS solution containing 10 mM 4-aminobenzoic acid, 100 μM Alexa Fluor™ 594 hydrazide (AF594-hydrazide), and 5% FBS for 60 min. For Apt and GO control sub-groups, Apt (10 μM) and GO (4.0 μM) was respectively used to replace A-G-SS-P, with other procedures identical to A-G-SS-P sub-group. After washing the bladders with PBS, the three sub-groups were sacrificed by cervical dislocation, and the bladders were harvested for imaging on IVIS Spectrum *in vivo* imaging system. The intensity of the *ex vivo* fluorescence signal was analyzed using Living Image® 4.7.3. For the muscle group, the operation procedure for each sub-group was the same as that for the corresponding one in the bladder group except eliminating the washing step due to the property of muscles.

Immunofluorescence co-localization assay of MUC1 cytoplasmic tail (MUC1-CT) and β-catenin

MCF-7 cells were seeded and cultured in serum-free medium overnight. After three-time washing with PBS and blocking, the cells were subjected to A-N-SS-P based LED treatment. Then the cells were treated with Siglec-9 (5 μg/mL in PBS) at 37 °C for 1 h, followed by fixation with 100% alcohol at r.t. for 5 min, and washing with ice-cold PBS. Next, the cells were permeabilized with 0.1% Triton X-100 at r.t. for 5 min, blocked with PBS containing 10% goat serum at 37 °C for 1 h, and incubated with a mixture of diluted anti-β-catenin antibody and anti-MUC1-CT antibody in PBST containing 1% BSA overnight at 4 °C. After washing three times with PBS, the cells were incubated with a mixture of diluted goat anti-rabbit IgG H&L (Alexa Fluor® 488) and goat anti-armenian hamster IgG H&L (Alexa Fluor® 647) in 1% BSA-containing PBST at r.t. for 1 h in the dark, respectively. The emission signals were collected from 505 nm to 550 nm and from 657 nm to 707 nm by CLSM under 495 nm and 647 nm excitation, respectively. The scatterplot images and Pearson's coefficients were obtained by using Leica Application Suite Advanced Fluorescence (LAS AF).

For comparison, (1) the cells without Sia trimming, (2) cells after global Sia trimming (treatment with 1.4 μM NEU at 37 °C for 30 min) and (3) cells only treated by TCEP (2 mM) at r.t. for 1 h, with and without Siglec-9 stimulation, were also respectively subjected to immunofluorescence co-localization assay as described above.

Cell migration assay

According to the standard procedure of in vitro scratch assay, MDA-MB-231 cells were seeded in six-well plates and cultured in RPMI-1640 cell medium for 48 h. After performing MUC1-specific or global Sia trimming, the cell monolayer was scraped by a sterile pipette tip when cells grew to 80% confluence, followed by washing three times with PBS to discard cell debris. Then the cells were incubated in serum-free medium for different time periods (0, 12, 24, and 36 h). With the migration of cells into the scratch region, images were acquired by an inverted fluorescence microscope, and the cell migration was evaluated by calculating the scratch closure distance using Image J software. For each image, the scratch distance was calculated through dividing the scratch area by the scratch length. The scratch closure distance was obtained by subtracting the scratch distance

Please cite this article in press as: S. Li et al., Materials Today (2021), https://doi.org/10.1016/j.mattod.2021.04.015

for different time periods from that for 0 h. To evaluate the influence from TCEP on cell migration, MDA-MB-231 cells after treatment by TCEP (2 mM) at r.t. for 1 h under gentle shaking were also subjected to in vitro scratch assay.

Results and discussion

Design principle for the pro-editing conjugate

For the initial proof-of-concept demonstration, MUC1-specific terminal Gal/GalNAc is selected as the carbohydrate unit to be edited. MUC1, an integral membrane glycoprotein bearing an extracellular, heavily *O*-glycosylated variable number tandem repeat (VNTR) domain, plays an important role in cell signaling, pathogen binding, and tumor progression [18]. Terminal Gal/GalNAc is a key structural motif governing the cellular physiological state and neoplastic process [19]. The glyco-editing probe is designed by integration of MUC1-targeting, terminal Gal/GalNAc-editing, molecular cloaking, and switch linker components into a single caged, pro-editing conjugate (Fig. 1a). The four modules adopted herein are, respectively, a high-affinity, MUC1-binding DNA aptamer S2.2 (Apt in abbreviation) [20], GO, PEG, and disulfide linker. The use of small-sized 25mer Apt instead of a large-sized antibody is to strictly ensure the confinement of glyco-editing event within MUC1 and thus contribute to the achievement of protein specificity. Moreover, the dynamic hybridization nature of aptamer [21] enables sequential docking and erasing of the conjugate, thus contributing to the cascading of multi-step localized glyco-editing manipulations. GO is an efficient enzyme permitting the transformation of C6-hydroxy group of terminal Gal/GalNAc to the aldehyde group [22,23], a bioorthogonal functionality amenable to further structural elaboration on cell surface. PEG can bind to a large pool of water molecules to create a ballooning-type conformation and a water barrier, thus effectively preventing a macromolecular substrate from accessing the catalytic center of an enzyme [24]. Disulfide bond is a chemically labile linkage that can be facilely cleaved in response to a variety of reducing triggers [25,26]; its privileged role as a switch derives from its orthogonality to other linker chemistry.

Preparation and characterization of the pro-editing conjugate A-G-SS-P

The pro-editing conjugate is constructed through a stepwise assembly protocol (Fig. 2a). Briefly, the surface-exposed amino groups of GO first react with the *N*-hydroxysuccinimide ester group of SPDP to afford G-SS; PEG terminated with a methoxy group and a thiol group at the chain ends (mPEG-SH; M. W. ~ 2000) (*vide infra*) is then coupled to G-SS via disulfide exchange to generate G-SS-P; further reaction between the amino group of 3′-amino-derivatized Apt (Apt-NH_2; all DNA sequences read from 5′ to 3′) and surface carboxyl groups of GO in G-SS-P provides the final pro-editing conjugate A-G-SS-P. The electrostatic interaction between Apt-NH_2 with negative charge and electropositive GO (with isoelectric point above pH 10), may facilitate their covalent conjugation. The successful production of G-SS and G-SS-P is unambiguously confirmed with matrix-assisted laser desorption/ionization time-of-flight mass spectrometry (MALDI-TOF MS, Fig. 2b). An apparent MS peak shift, from *m*/*z* 68,407 to *m*/*z* 69148, is observed upon the transformation of GO to G-SS, indicating the attachment of ~4 SPDPs per GO. Upon coupling formation of G-SS-P, four new peaks emerge at a regular shift interval of ~2000 and with a maximum value of m/z 77070, consistent with the mixture linking of 1, 2, 3, 4 PEG chains per GO; this is further supported by the sodium dodecyl sulfate–polyacrylamide gel electrophoresis (SDS-PAGE) analysis (Fig. 2c), showing four major up-shifted discrete bands for G-SS-P as compared to GO and G-SS (Fig. 2c, lane 4). The conjugation of Apt to G-SS-P (*vide infra*) is evidenced by a prominent UV–vis absorption peak at 260 nm (Fig. 2d); quantitative calculation gives ~3 Apt per GO; also, a slight downward shift of the major bands is witnessed for A-G-SS-P on SDS-PAGE in reference to those of G-SS-P (Fig. 2c, lane 5), likely reflecting the combined contribution of mass and charge from Apt.

Demonstration of the cloaking/uncloaking property of A-G-SS-P in vitro

With the pro-editing conjugate A-G-SS-P synthesized, the cloaking/uncloaking property with respect to the control of accessibility of GO is then evaluated. In principle, PEG is supposed to be capable of cloaking GO in catalytically incompetent state only for a macromolecular substrate. As expected, using small molecule Gal as the substrate, various GO conjugates show basically similar catalytic activity as GO (Fig. 2e and Fig. S1). This also excludes the influence of conjugation operation on enzyme activity. GO in A-G-SS-P is also accessible for catalysis to disaccharide substrate such as Lac (Fig. 2e). In contrast, a severely impaired GO catalytic activity of A-G-SS-P is detected for a macromolecular-sized, terminal Gal/GalNAc-bearing glycoprotein substrate MUC2; the PEG cloaking effect is also manifested in the minimal Gal/GalNAc-editing capability of A-G-SS-P for fixed MCF-7 cells. The caged, inaccessible GO in A-G-SS-P is designed to be decaged to the accessible state by the cleavage of disulfide bond and associated uncloaking release of PEG. This can be achieved with TCEP, a cell-compatible, highly potent and robust reducing trigger [26]. TCEP proves to have virtually no negative impact on the catalytic activity of GO and its conjugates (Fig. 2e and Fig. S1). The ability to cleave disulfide bond in G-SS-P and A-G-SS-P with TCEP is verified on SDS-PAGE by the disappearance of originally up-shifted bands and re-emergence of a single band at the approximate location of GO and G-SS (Fig. 2c, lanes 8 and 9). This TECP-triggered uncloaking of GO from A-G-SS-P can largely restore GO to the decaged, catalytically competent state for MUC2 and MCF-7 cells (Fig. 2e).

Protein-specific Gal/GalNAc editing on live cells

The feasibility of using pro-editing conjugate A-G-SS-P for live-cell protein-specific glyco-editing is next systematically examined on MUC1-positive MCF-7 cells. The editing of terminal Gal/GalNAc on cell surface by GO allows the generation of aldehyde as a reactive handle for ligation with FTZ [27], which can be imaged by CLSM and quantitated by cell periphery FI measurement. To stringently eliminate off-target Gal/GalNAc editing at the MUC1-targeting A-G-SS-P delivery stage, mPEG-SH loading is optimized at a GO concentration of 0.4 μM, based on the extent of GO cloaking and correspondingly, the degree of diminished GO editing capacity in G-SS-P, which identifies 1000 μM as the effective concentration (Fig. S2A and C). The necessity of using such a high mPEG-SH to GO molar ratio might be due to

Please cite this article in press as: S. Li et al., Materials Today (2021), https://doi.org/10.1016/j.mattod.2021.04.015

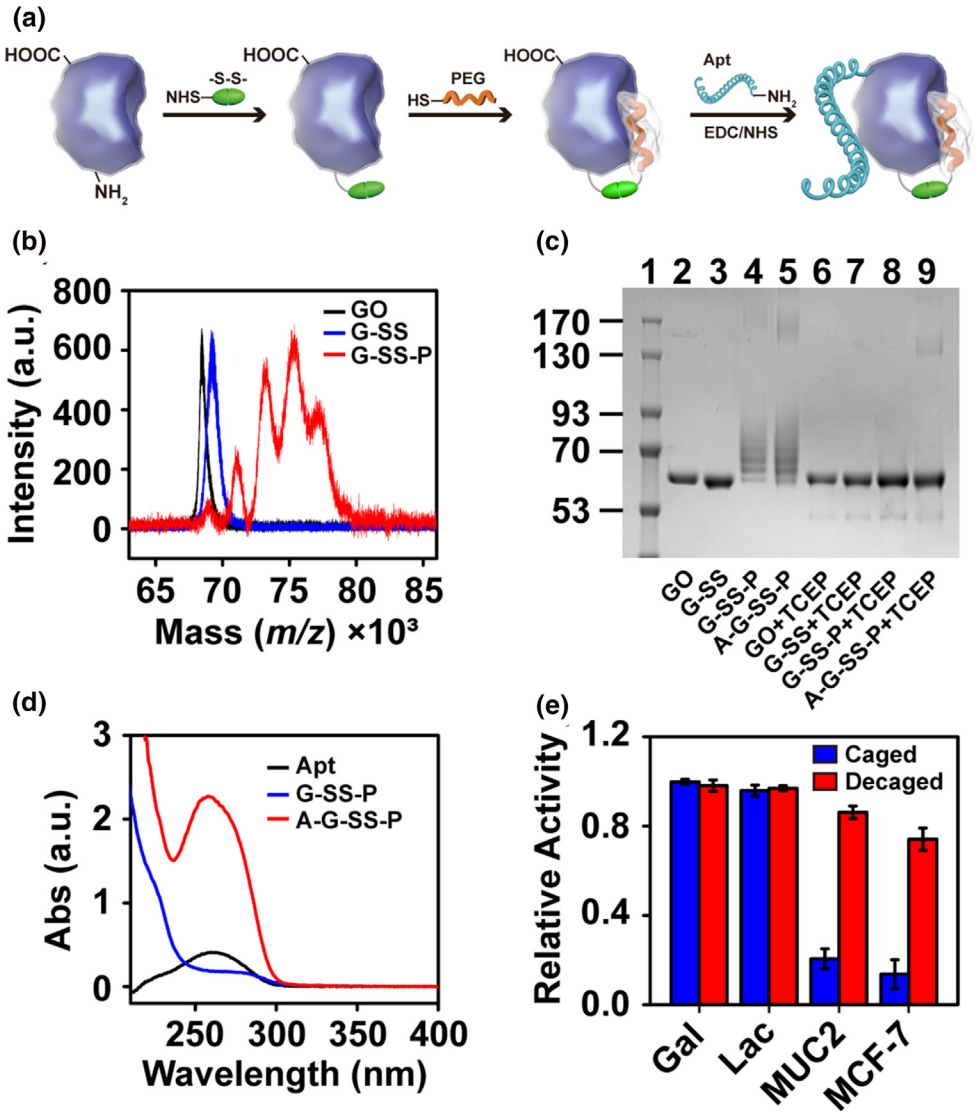

FIGURE 2

Characterization of A-G-SS-P *in vitro*. (a) Scheme for the preparation of the pro-editing conjugate A-G (N)-SS-P. The blue shape represents GO or NEU. (b) MALDI-TOF MS spectra of GO, G-SS, and G-SS-P. (c) SDS-PAGE analysis of GO, G-SS, G-SS-P, and A-G-SS-P before and after TCEP treatment, respectively (lanes 2–9), and lane 1 is protein ladder (10–180 kDa). (d) UV–vis spectra of Apt, G-SS-P, and A-G-SS-P. (e) Relative enzymatic activities of A-G-SS-P before (caged) and after (decaged) TCEP cleavage using Gal, Lac, MUC2, and fixed MCF-7 cells as substrates, respectively. For each type of substrates, the activity of GO of equivalent amount is set as 1. Data are means ± SD ($n = 3$).

the partial burial of thiol group by the long-chain, flexible PEG molecules. The chain length of mPEG-SH can also affect the cloaking outcome for GO; a ~2000 M.W. size proves to be adequate (Fig. S2B and D). Apt is single-stranded DNA that can potentially act as a steric barrier to block, unintendedly, the accessibility of GO when excessively conjugated to G-SS-P; its loading concentration can be maximally set at 1.0 μM without imposing notably negative effect for GO, as evaluated in the case of A-G (Fig. S3). Under above loading condition, the MUC1-targeting capability is fully retained for Apt in as-synthesized A-G-SS-P, as validated by the comparable MCF-7 cell periphery FI from the binding of FAM-Apt-NH_2 and FAM-A-G-SS-P (Fig. 3a). The MUC1 recognition specificity of Apt is further evidenced by the lack of Apt binding to MUC1-negative HepG2 cells [28] as well as the failure of a random-sequenced DNA to exhibit affinity for MCF-7 cells (Fig. 3a).

With all the required properties demonstrated for A-G-SS-P at the MUC1-targeting stage, subsequent MUC1-specific terminal Gal/GalNAc editing is then undertaken. An important feature of our LED system is the high cell compatibility (Fig. 3b), rendering it ideally suited for live cell settings. The uncloaking of GO from A-G-SS-P after its initial binding to MUC1 on MCF-7 cells can be effected by TCEP of 2.0 mM (Fig. S4A and B), and yields MUC1-localized A-G-S. The proximity catalysis by A-G-S and subsequent FTZ labeling permit the imaging analysis of MUC1-specific terminal Gal/GalNAc (Fig. 4a and c), which shows an obvious fluorescence at cellular periphery. The LED system features a short protocol time, with the whole editing process completed within ~2 h. To exclude the possibility of accidental induction of non-specific adsorption of FTZ onto cell surface by the disulfide cleavage step, SPDP, mPEG-SH, and TCEP are each individually added to cells prior to FTZ labeling, and no fluores-

Please cite this article in press as: S. Li et al., Materials Today (2021), https://doi.org/10.1016/j.mattod.2021.04.015

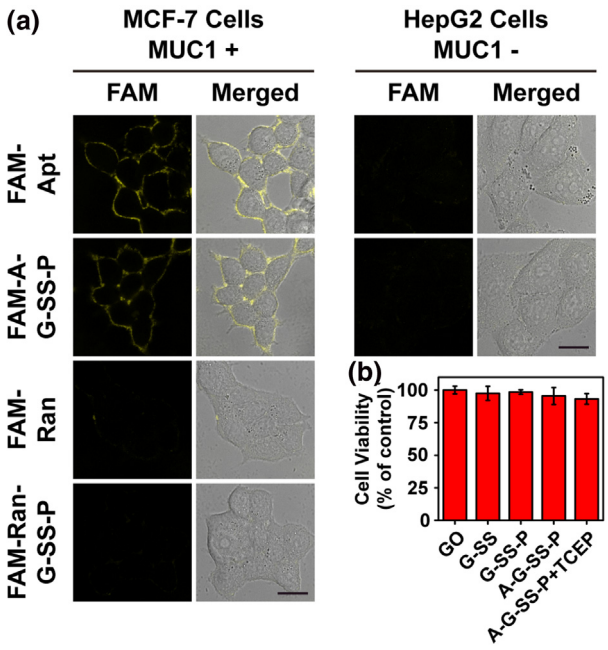

FIGURE 3

Demonstration of Apt binding specificity of A-G-SS-P toward MUC1 and cytocompatibility of various conjugates. (a) Demonstration of Apt binding specificity of A-G-SS-P toward MUC1. CLSM images of MCF-7 cells (MUC1+) and HepG2 cells (MUC1−) after incubation with FAM-Apt and FAM-A-G-SS-P, respectively, and MCF-7 cells after incubation with FAM-Ran and FAM-Ran-G-SS-P, respectively. Scale bars: 25 μm. (b) Cell viability of MCF-7 cells after treatment with GO, G-SS, G-SS-P, A-G-SS-P, and a mixture of A-G-SS-P and TCEP, respectively. Data are means ± SD (n = 3).

cence is observed (Fig. S4C). Both Apt binding and PEG cloaking are crucial for MUC1-specific Gal/GalNAc editing, as reflected in the loss of targeted editing capability for G-SS-P (the absence of aptamer results in its removal during the washing step and before the TCEP cleavage stage) and indiscriminate whole-cell surface editing of Gal/GalNAc in the case of A-G-SS (Fig. 4a and c).

Demonstration of the protein- and glyco-specificities

The MUC1-targeting specificity is also confirmed with the significantly lowered degree of editing upon the down-regulation of MUC1 expression level by a silencing shRNA (Fig. 4b and d) [28]. The terminal Gal/GalNAc-editing specificity is validated with three sets of experiments (Fig. 4b and d): (1) MUC1 is an *O*-glycosylated protein and inhibition of *O*-glycosylation pathway by benzyl 2-acetamido-2-deoxy-α-D-galactopyranoside (BAG) [29] indeed reduces editing to the background level. (2) Sia is a terminal carbohydrate moiety frequently capped over Gal/GalNAc and as expected, whole-cell Sia trimming enables the exposure of originally capped Gal/GalNAc to the terminal position, thus elevating the degree of editing. (3) The extra added Gal competes with MUC1-carried Gal/GalNAc, leading to incompetent editing. Glutathione (GSH) is an endogenous cellular species that possesses the reducing power for the cleavage of disulfide. However, no cell surface glyco-editing occurs in the presence of 20 μM GSH (Fig. S5), demonstrating that the typical extracellular GSH fluid concentration (2–20 μM) would not affect [30].

Protein-specific Sia trimming as a "loss-of-carbohydrate" model

To demonstrate the generic applicability of our LED strategy, MUC1-specific Sia trimming, as a "loss-of-carbohydrate" model, is pursued. Tumor-associated MUC1 has been reported to be highly sialylated, which causes premature termination of chain elongation and formation of truncated *O*-glycans [18]. This is also regarded as a common tumor-relevant glycosignature. The modular design of LED scheme allows the convenient adapted use of our established pro-editing conjugate synthesis protocol. Thus, NEU, a Sia-trimming enzyme [31], is analogously stepwise conjugated to SPDP, mPEG-SH, and Apt-NH_2 (*vide infra*). Consistent with the successful conjugation, MALDI-TOF MS reveals a consecutive shift of NEU MS peak position each after the SPDP and mPEG-SH coupling steps, corresponding to the formation of products N-SS and N-SS-P, respectively (Fig. 5a); SDS-PAGE displays a smeared band for both N-SS-P and pro-editing conjugate A-N-SS-P (Fig. 5b, lanes 4 and 5); a 260 nm UV–vis absorption band is also observed for A-N-SS-P (Fig. 5c). The numbers of SPDP, PEG, and Apt attached to each NEU in A-N-SS-P are calculated to be ~14, 5, and 3, respectively. The global sia trimming (GST) on cell surface can be visualized by attenuated cell periphery FI, using SNA-FITC as the Sia recognition lectin probe. The loading concentration of mPEG-SH is optimized to be 700 μM at a NEU concentration of 1.4 μM (Fig. S6A and C), based on the increment plateau FI from SNA-FITC; the sufficient value for mPEG-SH M.W. is again identified to be ~ 2000 (Fig. S6B and D); Apt can be loaded at a maximum concentration of 3.5 μM without blocking NEU (Fig. S7). The as-synthesized pro-editing conjugate A-N-SS-P exhibits highly selective targeting affinity for MCF-7 cell surface MUC1 (Fig. S8A), as verified by FAM-A-N-SS-P and the negative controls (FAM-Ran-N-SS-P and HepG2 cells). Accordingly, MUC1-specific Sia trimming can be achieved by initial MUC1-targeted binding of A-N-SS-P and subsequent LED by TCEP. However, the cell periphery FI from SNA-FITC staining, reflecting the total sialylation level on cell surface, can not provide statistically significant conclusion regarding the change of quantity of MUC1-bound Sia (MUC1-Sia), upon TCEP addition (Fig. 5d and e). Thus two additional sets of experiments are performed to validate MUC1-targeted Sia trimming. (1) Immunoprecipitation (IP) of MUC1 after MUC1-specific Sia trimming identifies a decreased quantity of MUC1-Sia by SNA blot analysis (Fig. 5f). The degree of Sia trimming on MUC1 is estimated to be 52.0% by calculating the ratio of LED-enabled decrease of MUC1-Sia signal to that by treatment with NEU in solution, assuming the achievement of complete cleavage by the latter protocol. The MUC1-Sia signal difference between the two trimming formats might arise from the limited pool of Sia available (due to, for example, steric hindrance and out-of-reach spatial distance) for MUC1-bound NEU. (2) Considering the exposure of underlying Gal/GalNAc by MUC1-specific Sia trimming, we use a previously established Fe^{II}/Fe^{III}-based inactivation/activation remodeling method for MUC1-specific terminal Gal/GalNAc [14] to evaluate the change of MUC1-Sia level. To achieve this, after performing Sia trimming with A′-N-SS-P/TCEP (i.e. 1^{st} glyco-editing, A′ is an extended Apt-bearing DNA

Please cite this article in press as: S. Li et al., Materials Today (2021), https://doi.org/10.1016/j.mattod.2021.04.015

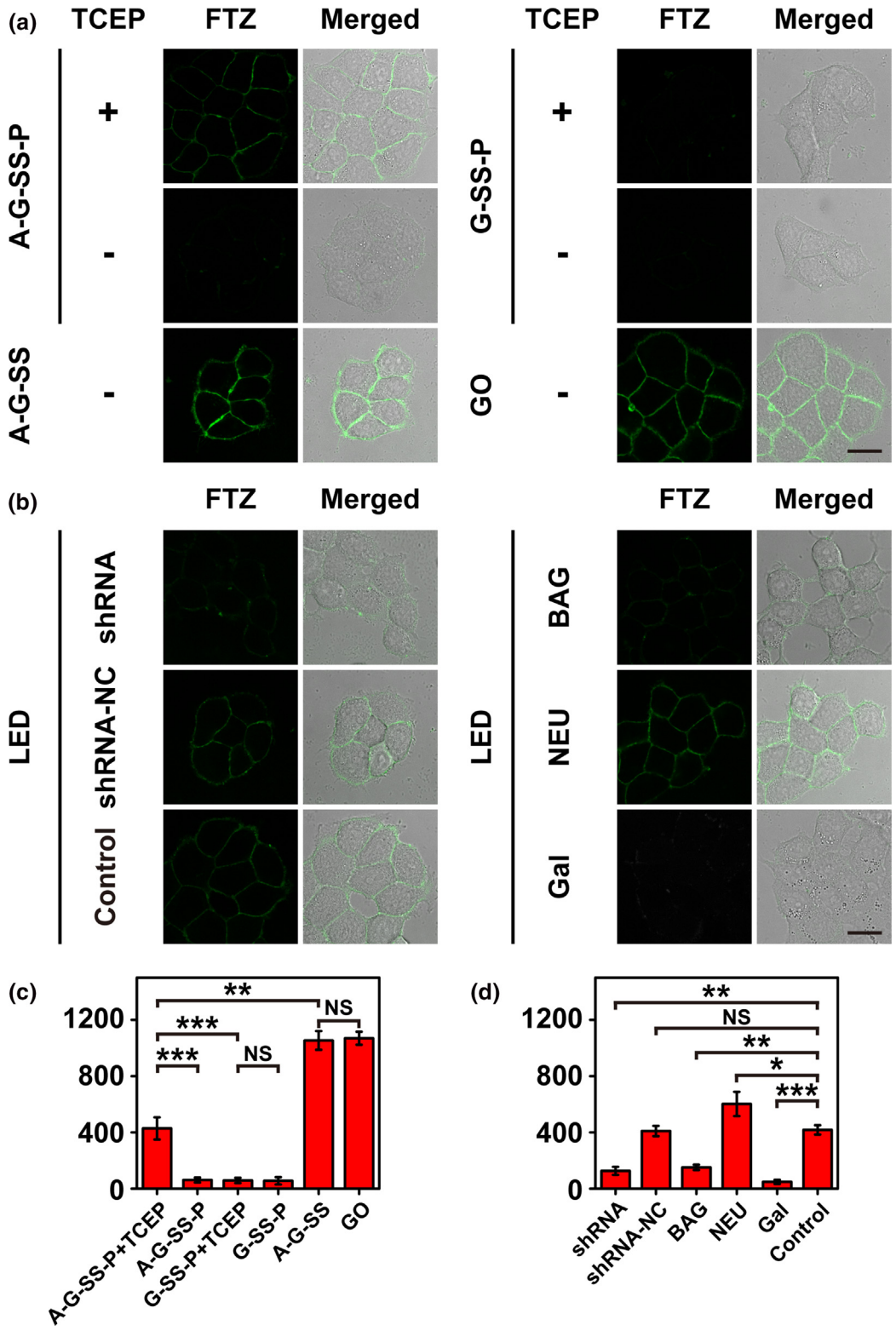

FIGURE 4

MUC1-specific terminal Gal/GalNAc editing on live MCF-7 cells by LED strategy. (a) CLSM images of MCF-7 cells after incubation with A-G-SS-P or G-SS-P, with and without subsequent TCEP treatment, and final FTZ labeling. Cells after treatment with A-G-SS or GO are also labeled with FTZ and imaged for comparison. (b) Demonstration of protein and glycan editing specificities of LED system by MUC1 down-regulation experiments (left), and glycosylation pathway disruption, whole-cell terminal Sia trimming and Gal competition experiments (right), respectively. Scale bars: 25 μm. (c) FI from (a). (d) FI from (b). Data are means ± SD ($n = 3$). Statistical significance was determined by unpaired two-tailed Student's *t*-test (*$P < 0.05$; **$P < 0.01$; ***$P < 0.001$; NS, not significant).

Please cite this article in press as: S. Li et al., Materials Today (2021), https://doi.org/10.1016/j.mattod.2021.04.015

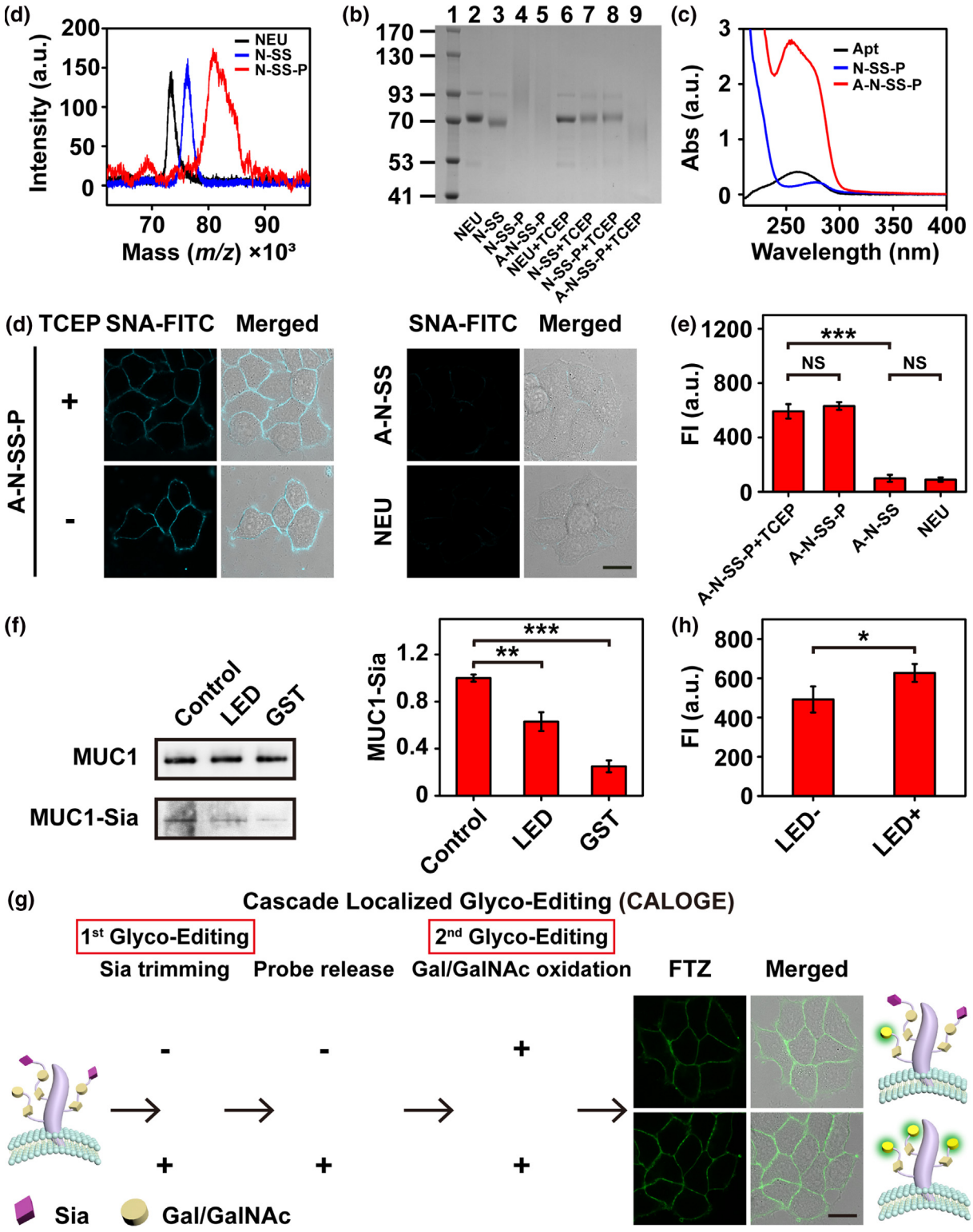

FIGURE 5

MUC1-specific Sia trimming on live MCF-7 cells by LED strategy. (a) MALDI-TOF MS spectra of NEU, N-SS and N-SS-P. (b) SDS-PAGE analysis of NEU, N-SS, N-SS-P, and A-N-SS-P before and after TCEP treatment, respectively (lanes 2–9), and lane 1 is protein ladder (10–180 kDa). (c) UV–vis spectra of Apt, N-SS-P, and A-N-SS-P. (d) CLSM images of MCF-7 cells after incubation with A-N-SS-P, with and without subsequent TCEP treatment, and final SNA-FITC labeling. Cells after treatment by A-N-SS or NEU are also labeled with SNA-FITC and imaged for comparison. Scale bar: 25 μm. (e) FI from (d). (f) Verification of MUC1-Sia expression decrease after LED or global Sia trimming (GST) treatment by immunoprecipitation of MUC1 followed by anti-MUC1 antibody and SNA blotting. The red columns show the greyscale values from the blot. (g and h) Demonstration of MUC1-targeted Sia trimming by cascade localized glyco-editing (CALOGE). (g) For cells after Sia-trimming with A′-N-SS-P/TCEP, A′-comp is added to release A′-N-S. Then treated and untreated cells are respectively subjected to G-A (inactivated by $K_4[Fe(CN)_6]$) incubation, $K_3[Fe(CN)_6]$ activation, FTZ reaction and CLSM imaging. Scale bar: 25 μm. (h) FI from (g). Data are means ± SD ($n = 3$). Statistical significance is determined by unpaired two-tailed Student's *t*-test (*$P < 0.05$; **$P < 0.01$; ***$P < 0.001$; NS, not significant).

Please cite this article in press as: S. Li et al., Materials Today (2021), https://doi.org/10.1016/j.mattod.2021.04.015

strand designed to be amenable to toehold-mediated strand displacement), the MUC1-bound A′-N-S is released by strand displacement hybridization with a complement strand of A′ (A′-comp, this aptamer-erasing step leads to probe release). Then a MUC1-specific Gal/GalNAc remodeling probe, G-A with GO inactivated by $K_4[Fe(CN)]_6$, is guided to MUC1 by Apt recognition. After washing, the GO is activated by $K_3[Fe(CN)_6]$ to execute Gal/GalNAc oxidation (i.e. 2nd glyco-editing), thus enabling FTZ labeling for fluorescence observation (Fig. 5g). An increased quantity of MUC1-specific terminal Gal/GalNAc is observed when compared with the group without pretreatment by LED-based Sia trimming (Fig. 5h). Of particular note, the Fe^{II}/Fe^{III}-based inactivation/activation remodeling method is limited to GO [32], and is not generally applicable to other glyco-enzymes. This result not only demonstrates MUC1-targeted Sia trimming, but also suggests a unique property of the LED strategy: the aptamer-based conjugate can be released to recover the recognition capability of target protein (through dynamic DNA strand displacement principle), thus enabling the achievement of CALOGE manipulations by sequentially using different glyco-enzymes for the generation of complex, artificially designer protein-specific glycoform. In addition, the MUC1-specific Sia trimming LED system also features high cell compatibility (Fig. S8B), and the non-specific interference with SNA-FITC from the disulfide cleavage has also be ruled out by control experiments on SPDP, mPEG-SH, and TCEP (Fig. S9). The critical modular importance of PEG cloaking is again echoed by the indiscriminate whole-cell surface Sia trimming in the case of A-N-SS (Fig. 5d and e).

Protein-specific Gal/GalNAc editing in vivo

The achievement of glyco-editing on live cells encourages us to assess the feasibility of performing protein-specific glyco-editing *in vivo*. To demonstrate the protein-specificity, bladder (MUC1-positive) and thigh muscles (MUC1-negative) of live, female C57BL/6J mice, are chosen as the *in vivo* editing objects (Fig. S10). The binding specificity of Apt toward murine MUC1 is confirmed by the obvious binding signal when directly incubating Alexa Fluor™ 594 modified Apt (AF594-Apt) with MUC1-positive murine bladder, and the negligible fluorescence when pre-blocking MUC1 epitopes with anti-MUC1 antibody (Fig. S11). Bladder irrigation and intramuscular injection are respectively used for reagent administration to murine bladders and muscles. For either type of editing objects, three sub-groups of experiments are designed: the mice are administered 1) A-G-SS-P, 2) Apt (as negative control) or 3) GO (as positive control), followed by TCEP treatment and AF594-hydrazide labeling. Then the bladder and muscle tissues are harvested for *ex vivo* fluorescence observation, and the signals from AF594 reflect the editing efficacy. As can be seen in Fig. 6, the bladders after A-G-SS-P based LED treatment exhibit obvious fluorescence just as the GO sub-group does, while Apt sub-group displays indiscernible signal. However, in MUC1-negative muscles, A-G-SS-P sub-group shows negligible signal, indicating that in the absence of MUC1 expression in muscles, the rapid diffusion of A-G-SS-P from muscles leads to incompetent Gal/GalNAc editing. While administration of GO can still generate relatively weak fluorescence signals, as compared with those in the corresponding bladder group. These data demonstrate that protein-specific glyco-editing can be achieved by the proposed LED strategy in complex *bona fide* biological environments.

Investigation of the effects of MUC1-Sia on Siglec-9-mediated signal transduction

Live-cell protein-specific glyco-editing provides an unprecedented opportunity to directly link a biological effect with a particular protein glycoform. It has been reported that a Sia-binding immunoglobulin-like lectin, Siglec-9, can interact with MUC1-Sia to activate MUC1-CT cleavage and associated recruitment of β-catenin to cytoplasm and nucleus [33,34]. However, this has never been verified on native MUC1 in situ. In this context, we perform MUC1-specific Sia trimming on MCF-7 cells, and compare the immunofluorescence from anti-β-catenin and anti-MUC1-CT antibody staining with that of cells untrimmed or after GST in the presence and absence of Siglec-9 (Fig. 7a and Fig. S12). For cells without Sia trimming (control), upon Siglec-9 addition, a notably increased colocalization ratio of the two proteins can be observed, as well as the transport of β-catenin from cell membrane to cytoplasm (major portion) and nucleus (minor portion); whereas without Siglec-9 stimula-

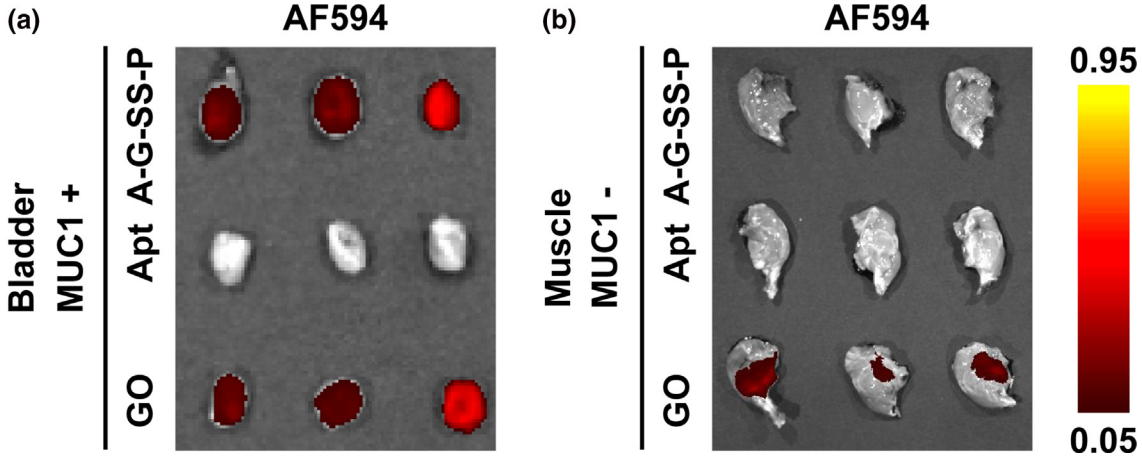

FIGURE 6

Ex vivo fluorescence images of (a) bladder and (b) muscle tissues after performing *in vivo* glyco-editing. The mice are sequentially treated with A-G-SS-P (or Apt, GO), TCEP and AF594-hydrazide by bladder irrigation or intramuscular injection before sacrifice.

Please cite this article in press as: S. Li et al., Materials Today (2021), https://doi.org/10.1016/j.mattod.2021.04.015

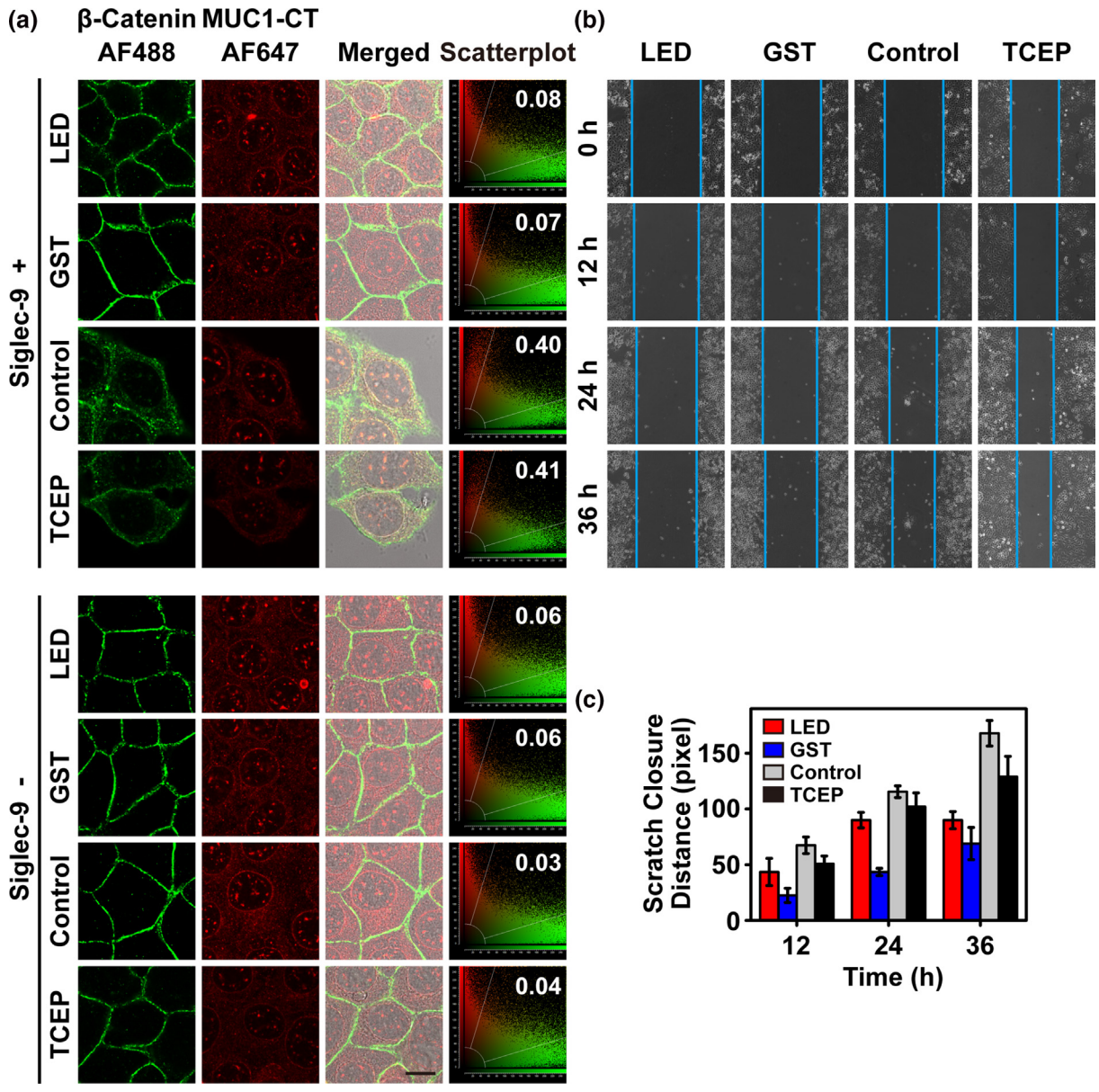

FIGURE 7

Investigation of the effects of MUC1-Sia trimming on cellular signaling and behavior. (a) Demonstration of the effect of MUC1-specific or global Sia trimming on the colocalization of β-catenin (green) and MUC1-CT (red) in MCF-7 cells in the presence and absence of Siglec-9 stimulation. The cells without treatment or undergoing only TCEP treatment are also stained with the two types of antibodies. Pearson's correlation coefficients are shown in the colocalization scatterplots. Scale bar: 16 μm. (b) Monitoring of the migration of MDA-MB-231 cells after MUC1-specific or global Sia trimming by scratch assay. Untreated cells and cells after TCEP treatment are also assayed for comparison. (c) Scratch closure distance along with migration time. Data are means ± SD (n = 3).

tion, β-catenin shows little association with MUC1-CT as reflected by the unambiguous green fluorescence at the periphery of cell membrane. However, for cells after MUC1-specific (or global) Sia trimming, the cytoplasmic/nuclear accumulation of β-catenin is largely (or completely) blocked regardless of the addition of Siglec-9, thus indicating the participation of MUC1-Sia in Siglec-9-mediated signal transduction pathways. The observed difference in β-catenin transport, with and without MUC1-specific Sia trimming, is not caused by TCEP, as demonstrated in Fig. 7a. These results demonstrate the compelling feature of our method: enabling the direct observation of glycans' functional roles on cellular signaling in a protein-specific manner.

Revelation of the role of MUC1-Sia on cell migration

Considering the prominent position of MUC1-Sia on cell membrane, we further apply our method to reveal the effect of MUC1-Sia on cell migration by in vitro scratch assay using MDA-MB-231 cells, a cell line with high metastatic capability, as the model (Fig. 7b). Compared with the untreated cells (Control group) and TECP-treated cells (TCEP group), retarded migration of MDA-MB-231 cells is observed accompanying MUC1-

Please cite this article in press as: S. Li et al., Materials Today (2021), https://doi.org/10.1016/j.mattod.2021.04.015

specific Sia trimming (LED group): the migration distance, as reflected by scratch closure distance, after 36-h incubation is 54% of that for untreated cells, and comparable to that for GST group (Fig. 7c) [35,36], demonstrating the critical role played by MUC1-Sia in cell migration.

Conclusion

In conclusion, a localized, live-cell glyco-editing probe has been developed for protein-specific revelation and manipulation of biological functions of glycans. The probe integrates a small-sized, target-recognition motif, i.e. aptamer, and an off–on switch mechanism of enzyme catalytic center's accessibility, i.e. PEG-based molecular cloaking/uncloaking scheme, on the glyco-editing enzyme. The great significance of the regulatory handle lies in four aspects: (1) Non-targeted editing is precluded during targeting stage, thus contributing to a spatial control; (2) A temporal control of the editing event is achieved with the off–on switch; (3) General adaptability to diverse glyco-editing enzymes (single-substrate or double-substrate) and thus to diverse glyco-editing scenarios (gain-of-carbohydrate, transformation-of-carbohydrate and loss-of-carbohydrate); (4) *In vivo* protein-specific glyco-editing is realized, which represents an important development of glyco-editing tools. The unique feature of our LED strategy is further manifested in the ability to achieve complex multi-step CALOGE manipulations, thus enabling facile and versatile remodeling of glycoforms on a particular protein.

Most importantly, our design allows direct observation of the functional role of glycans of a particular protein while avoiding the unnecessary perturbation on glycoforms of other proteins. This is a challenging-to-achieve goal for current glyco-editing approaches due to the lack of protein-targeting instrument. Unprecedented insight has been gained accordingly with respect to the effect of precision MUC1-targeted Sia trimming on cellular signaling and behavior. These discoveries suggest the probe as a generic investigation tool for revealing the biological consequences and manipulating the biological functions derived from protein-specific glyco-editing.

Data availability

The authors declare that the data supporting the findings of this study are available within the paper and SI, as well as from the authors upon request.

CRediT authorship contribution statement

Siqiao Li: Conceptualization, Methodology, Investigation, Writing - original draft, Writing - review & editing. **Anwen Mao:** Methodology, Investigation, Validation, Writing - review & editing. **Fan Huo:** Methodology, Investigation, Validation, Writing - review & editing. **Xiaojian Wang:** Supervision, Methodology, Investigation, Writing - review & editing. **Yuna Guo:** Methodology, Writing - review & editing. **Lu Liu:** Methodology, Writing - review & editing. **Chao Yan:** Supervision, Writing - review & editing. **Lin Ding:** Supervision, Conceptualization, Writing - original draft, Writing - review & editing. **Huangxian Ju:** Supervision, Writing - review & editing.

Declaration of Competing Interest

The authors declare that they have no known competing financial interests or personal relationships that could have appeared to influence the work reported in this paper.

Acknowledgments

We gratefully acknowledge support from the National Natural Science Foundation of China (21974067, 21675082, 21708019), the National Key Research and Development Program of China (2018YFC1004704), the Natural Science Foundation of Jiangsu (BK20170987), and the Fundamental Research Funds for the Central Universities (020514380184).

Appendix A. Supplementary data

Supplementary data to this article can be found online at https://doi.org/10.1016/j.mattod.2021.04.015.

References

[1] A. Varki, Glycobiology 27 (2017) 3–49.
[2] F. Bard, J. Chia, Trends Cell Biol. 26 (2016) 379–388.
[3] C. Xu, D.T.W. Ng, Nat. Rev. Mol. Cell Biol. 16 (2015) 742–752.
[4] C.R. Shurer et al., Cell 177 (2019) 1757–1770.
[5] S.S. Pinho, C.A. Reis, Nat. Rev. Cancer 15 (2015) 540–555.
[6] D.D. Engle et al., Science 364 (2019) 1156–1162.
[7] E. Saxon, C.R. Bertozzi, Science 287 (2000) 2007–2010.
[8] N. Nischan, J.J. Kohler, Glycobiology 26 (2016) 789–796.
[9] M.K. Shim et al., Angew. Chem. Int. Ed. 55 (2016) 14698–14703.
[10] Y. Ding et al., Plos One 10 (2015) e0116402.
[11] T.Q. Zheng et al., Angew. Chem. Int. Ed. 50 (2011) 4113–4118.
[12] J.-L. Chaubard et al., J. Am. Chem. Soc. 134 (2012) 4489–4492.
[13] H. Jiang et al., Angew. Chem. Int. Ed. 57 (2018) 967–971.
[14] J.J. Hui et al., Angew. Chem. Int. Ed. 56 (2017) 8139–8143.
[15] X. Yang et al., J. Am. Chem. Soc. 141 (2019) 3782–3786.
[16] L. Cheng et al., Angew. Chem. Int. Ed. 58 (2019) 7728–7732.
[17] C. Barber et al., J. Biol. Chem. 281 (2006) 17276–17285.
[18] S. Nath, P. Mukherjee, Trends Mol. Med. 20 (2014) 332–342.
[19] E. Rodríguez et al., Nat. Rev. Immunol. 18 (2018) 204–211.
[20] M. Yousefi et al., Biosens. Bioelectron. 130 (2019) 1–19.
[21] L. Li et al., J. Am. Chem. Soc. 141 (2019) 17174–17179.
[22] K. Parikka et al., J. Mol. Catal. B 120 (2015) 47–59.
[23] T.N.C. Ramya et al., Glycobiology 23 (2013) 211–221.
[24] A.J. Keefe, S.Y. Jiang, Nat. Chem. 4 (2012) 60–64.
[25] J. Zhou et al., Angew. Chem. Int. Ed. 58 (2019) 5236–5240.
[26] H. Kim et al., J. Am. Chem. Soc. 140 (2018) 1199–1202.
[27] P. Zhang et al., Chem. Eur. J. 25 (2019) 10505–10510.
[28] S.Q. Li et al., Angew. Chem. Int. Ed. 57 (2018) 12007–12011.
[29] A. Paszkiewicz-Gadek et al., Int. J. Mol. Med. 17 (2006) 669–674.
[30] R. Cheng et al., J. Control. Release 152 (2011) 2–12.
[31] N. Juge et al., Biochem. Soc. Trans. 44 (2016) 166–175.
[32] G.A. Hamilton et al., J. Am. Chem. Soc. 100 (1978) 1899–1912.
[33] R. Beatson et al., Nat. Immunol. 17 (2016) 1273–1281.
[34] S. Tanida et al., J. Biol. Chem. 288 (2013) 31842–31852.
[35] H. Cui et al., Oncol. Rep. 25 (2011) 1365–1371.
[36] S. Bassagañas et al., Pancreas 43 (2014) 109–117.

Please cite this article in press as: S. Li et al., Materials Today (2021), https://doi.org/10.1016/j.mattod.2021.04.015